Structural Engineering and Mechanics, *Vol. 71, No. 6 (2019) 751-761*
DOI: https://doi.org/10.12989/sem.2019.71.6.751

Quantitative evaluation of through-thickness rectangular notch in metal plates based on lamb waves

Na Zhao[1], Bin Wu[1], Xiucheng Liu[1], Keqin Ding[2], Yanan Hu[2] and Mahmoud Bayat *[3]

[1]*College of Mechanical Engineering and Applied Electronics Technology, Beijing University of Technology, Beijing, China*
[2]*China Special Equipment Inspection and Research Institute, Beijing, China*
[3]*Department of Civil and Environmental Engineering, University of Pittsburgh, 3700 O'Hara Street, 729 Benedum Hall, Pittsburgh, PA 15261, USA*

(Received March 26, 2016, Revised July 16, 2019, Accepted August 26, 2019)

Abstract. Lamb wave technology is a promising technology in the field of structural health monitoring and can be applied in the detection and monitoring of defects in plate structures. Based on the reconstruction algorithm for the probabilistic inspection of damage (RAPID), a Lamb-based detection and evaluation method of through-thickness rectangular notches in metal plates was proposed in this study. The influences of through-thickness rectangular notch length and the angle between sensing path and notch length direction on signals were further explored through simulations and experiments. Then a damage index calculation method which focuses on both phase and amplitude difference between detected signals and baseline signals was proposed. Based on the damage index difference between two vertically crossed sensing paths which pass through the notch in a sensor network, the notch direction identification method was proposed. In addition, the notch length was determined based on the damage index distribution along sensing paths. The experimental results showed that the image reconstructed with the proposed method could reflect the information for the evaluation of notches.

Keywords: lamb waves; through-thickness rectangular notch; piezoelectric transducers; reconstruction algorithm for the probabilistic inspection of damage

1. Introduction

Vibration is one of the principal characteristics of any structure such as beam, paltes, shell, etc. To capture the real behavior of any structures, firstly, the governing equations of the problems are developed, and the different mathematical procedure is studied for solving them (Samaee *et al.* 2015, Delkhosh *et al.* 2018, Avazpour, 2018, Avazpoura *et al.* 2016, Jamshidi *et al.* 2012, Hashemiparast *et al*.2008).

Plate-like or plate structures are widely applied in aerospace, marine, chemical, mechanical and other fields. Plates are subjected to load shock, stress concentration and environmental factors, which can easily cause fatigue damage, affect the performance of the entire structure and sometimes lead to catastrophic consequences. Methods of damage detection in plate-like structures have attracted increasing attention in the past decade (Cao *et al.* 2013, Xu *et al.* 2013,2015,2019a,2019b). Lamb waves are ultrasonic guided waves propagating in the plate-like structure and have the characteristics of small attenuation, long propagation distance and high sensitivity to small damages. Lamb wave method is the most promising non-destructive testing method and can realize large-scale detection and monitoring of defects in plate structures (Su *et al*. 2006, Rose 2002, Ihn and Chang 2004, Hong *et al*. 2014, Ng 2015).

However, due to the complexity of Lamb wave propagation, when Lamb waves encounter a defect, reflection, refraction and mode conversion occur, thus making it difficult to identify and evaluate a defect with Lamb wave-based methods. Detection methods based on Lamb waves are mainly pulse-echo and pitch-catch methods (Sohn and Krishnaswamy 2004, Santos *et al*. 2008). The interactions between lamb waves and fatigue damages were extensively explored (Lee and Staszewski 2003, Lu *et al*. 2017). Lowe *et al*. (2002a, b) explored the scattering features of S0 and A0 mode Lamb at a rectangular notch and indicated the relationship between the changes in rectangular notch width and depth and the reflection coefficients. Lu *et al*. (2007, 2008) determined the through-thickness crack direction and length in aluminum plate by studying the changes in reflection and transmission coefficients when Lamb waves in different incident angles encountered a defect. Lu *et al*. (2008), Yang *et al*. (2016) and He *et al*. (2017) realized the length detection of a crack in plate-like structures by combining finite element simulation with the Bayesian method. Liu *et al*. (2018) and Fan *et al*. (2018) used the Lamb wave wavenumber approach to characterize the defects in an isotropic thin plate. Ghadami *et al*. (2015) used combined pulse-echo and pitch-catch methods to identify rectangular notch parameters in a plate using Lamb waves. Sen *et al*. (2017) developed a statistical learning-based approach for damage detection in beams through the inherent sparsity.

*Corresponding author, Researcher
E-mail: mbayat14@yahoo.com; mab609@pitt.edu

ISSN: 1225-4568 (Print), 1598-6217 (Online)

For the damage detection in plate-like structures, two sensors can only determine a particular trajectory at the defect, but the defect position cannot be accurately determined. The Lamb wave technology-based on multi-sensor array can realize the positioning and imaging of defects in plate-like structures. Deraemaeker *et al*. (2010) summarized the design and optimization of appropriate sensor networks, training of machine learning techniques and multi-scale approaches for dealing with local damage. Common defect imaging algorithms include damage imaging algorithm based on triangulation algorithm, tomography imaging algorithm, and reconstruction algorithm for the probabilistic inspection of damage (RAPID) (Lu *et al*. 2006, Rucka *et al*. 2018, Eugenio *et al*. 2018, Rao *et al*. 2017, Huang *et al*. 2014). Based on the difference in time of flight of scattered signals of Lamb waves at sensors, Su *et al*. (2006) determined the defect position in aluminum plates with the triangulation method. Rao *et al*. (2017) obtained the thickness image of corrosion damages by using a reconstruction algorithm based on full waveform inversion (FWI). Ng (2015) used cross-correlation of the wavelet coefficient and the Lamb wave diffraction tomography to evaluate the size and depth of corrosion damages. Wang *et al*. (2010) combined a damage diagnostic imaging algorithm with Shannon-entropy-based interrogation to identify surface damage in a stiffener-reinforced CF/EP quasi-isotropic woven laminate. Lee *et al*. (2015) presented the guided wave tomographic imaging for crack detections and visualization by the RAPID algorithm. Velsor *et al*. (2007) predicted defect location and severity in steel pipes by employing the RAPID algorithm based on the guided wave. Liu *et al*. (2015) combined the virtual time-reversal method with the RAPID and realized the detection imaging of delamination in composite plates without baseline signals. Wang *et al*. (2014, 2016) evaluated the direction and length of cracks along the sensing path with the RAPID based on correlation analysis. Among them, the RAPID is a weighted distribution imaging algorithm based on correlation coefficients proposed by the Rose Team of the University of Pennsylvania, USA (Zhao *et al*. 2007, Yan *et al*. 2010). The method does not require to know wave velocity and is applicable to monitor large-area structures. In this study, the variations of scattered signals of Lamb waves at a through-thickness rectangular notch (hereinafter referred to as notch) in an aluminum plate were studied by finite element analysis and experiments. In addition, the damage index calculation method was proposed for notch characterization. Based on the various characteristics of damage index obtained under different angles between sensing path and notch length direction, the identification method of notch direction was proposed. Finally, notch positioning and evaluation was performed with the improved RAPID.

2. Influences of Notch Parameters on Received Signals

Finite element analysis was combined with experiments to analyze the influences of notch length change on received signals and the influences of different angles between sensing path and notch length direction on received signals.

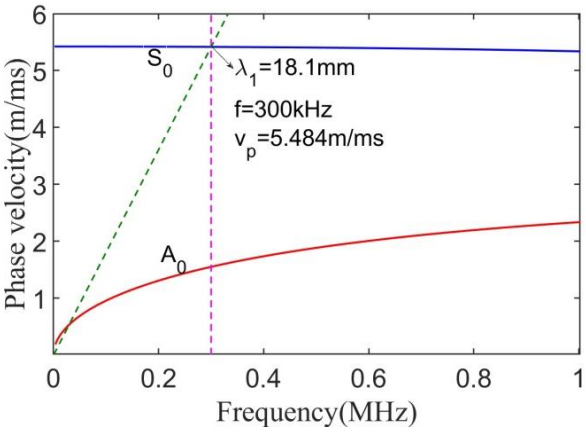

(a) Phase velocity

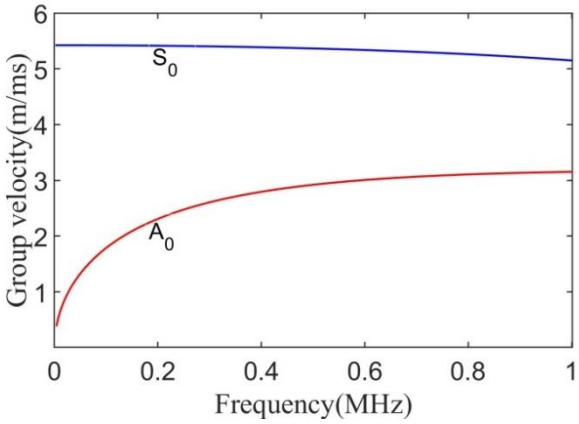

(b) Group velocity

Fig. 1 Dispersion curves in a 1-mm-thick

2.1 Finite Element Analysis

Abaqus software is a finite element modeling software and characterized by strong analytical ability and high reliability (Moser *et al*. 1999). In this study, Abaqus software was used to study the propagation behavior of Lamb waves in plate structures containing notches. The simulation was carried out with an aluminum plate (1000 mm*1000 mm*1 mm). The mechanical properties of the aluminum plate are provided in Table 1 and the dispersion curve is shown in Fig. 1. The adopted excitation wave is a five-cycle sinusoidal tone burst modulated by a Hanning window:

$$u(t) = A[H(t) - H(t - n/f_c)](1 - \cos\frac{2\pi f_c t}{n})\sin(2\pi f_c t) \quad (1)$$

where A is the amplitude; f_c is the center frequency; n is the number of the cycles; H is Heaviside function.

According to the dispersion curve of the aluminum plate shown in Fig. 1, there are two modes of Lamb waves at low frequency: the symmetric mode S0 and the anti-symmetric mode A0. The selected excitation frequency is 300 KHz and the excitation waveform is shown in Fig. 2. The group

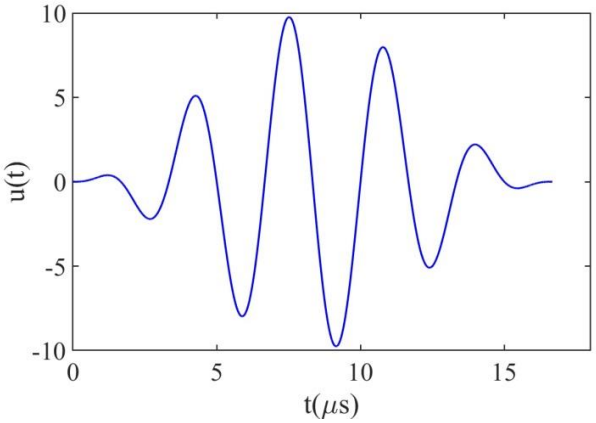

Fig. 2 Excitation waveform

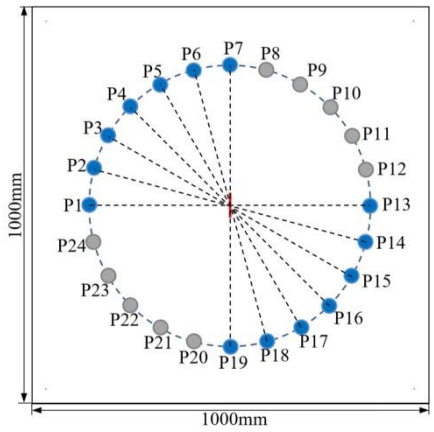

Fig. 3 Sensor layout

Table 1 Mechanical properties of the aluminum plate

Material	ρ (kg/m^3)	E(GPa)	σ
Aluminum	2700	70	0.34

velocity of the S0 mode is about 5500 m/s, whereas the group velocity of the A0 mode is about 2700 m/s.

The study focuses on the relationship between direct waves and notch changes. The first mode that arrives at the reception point is the symmetric mode S0. Since the distance between the reception point and the edge of the aluminum plate was more than 300 mm, the boundary reflection wave did not overlap with the mode S0. Therefore, in the simulation, vertical and opposite concentrated forces of 10 N were applied on the upper and lower symmetric points of the aluminum plate to generate the symmetric mode S0 in the plate.

In finite element modeling, the element size is related to the calculation accuracy. The principle for element setting is that a Lamb wave wavelength spans at least 10 elements to ensure calculation accuracy and convergence. As shown in Fig. 1, the phase velocity C of the S0 mode at the excitation frequency of 300 kHz is 5484 m/s and the minimum wavelength is:

$$\lambda_{\min} = \frac{C}{f_{\max}} = \frac{5484}{300\times10^3} m = 18.28mm \tag{2}$$

The maximum element size is:

$$L_{\min} \langle \frac{\lambda_{\min}}{10} = 1.828mm \tag{3}$$

The thickness of the aluminum plate should be an integral multiple of the element size. Considering the calculation speed and accuracy, the element size was set at 0.5 mm.

2.1.1 Influences of notch length on simulation signals

A through-thickness rectangular notch with a width of 0.2 mm was simulated at the center of the aluminum plate and the notch length ranged from 0 mm to 60 mm with a step size of 5 mm. The excitation-reception points were located at symmetric positions (P1 and P13) on both sides of the notch and the distance between excitation and reception points was set as 400 mm (Fig. 3). The simulation results are shown in Fig. 4. With the increase in notch length, the signal amplitude gradually decreased and the phase-shifted to the right.

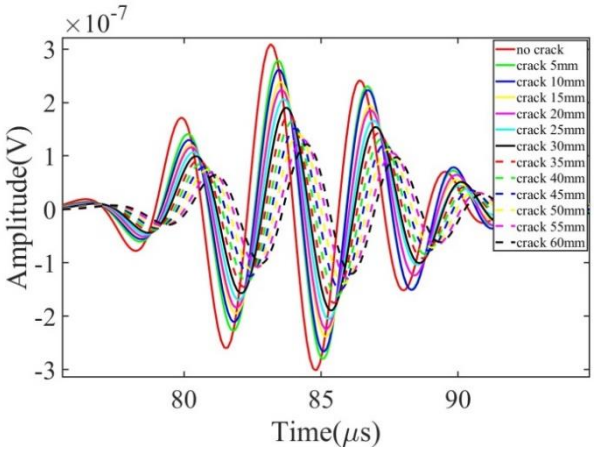

Fig. 4 Simulation signals of notches with different lengths

2.1.2 Influences of angle between sensing path and notch length direction on simulation signals

When Lamb waves passed through the notch at different angles, the obtained scattered fields were different. The influences of different angles on received signals were studied. The simulated signals of the reception points in the paths P7-P19(angle=0°), P6-P18(angle=15°), P5-P17(angle=30°), P4-P16(angle=45°), P3-P15(angle=60°), P2-P14(angle=75°) and P1-P13(angle=90°) shown in Fig. 3 were explored. In the above settings, under the constant propagation distance, the angle between sensing path and notch length direction increased from 0° to 90° with the step of 15°. In order to make the results more convincing, two notches with a width of 0.2 mm and the lengths of 30 mm and 60 mm were simulated respectively at the centers of two aluminum plates. The simulation results are shown in Fig. 5.

For the 30-mm long notch (Fig. 5(a)), when the angle between sensing path and notch length direction increased from 0° to 60°, the amplitude of simulated signals gradually decreased and the phase-shifted to the right. When the angle

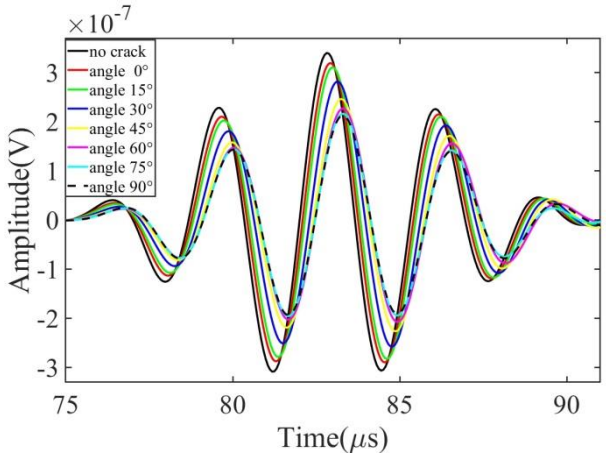

(a) Simulation signal under the 30-mm long notch

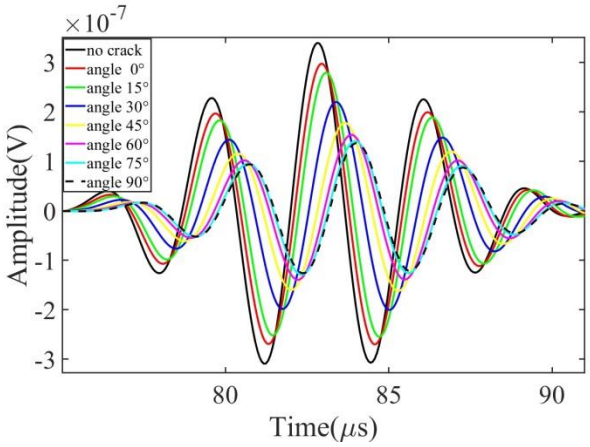

(b) Simulation signal under the 60-mm long notch

Fig. 5 Simulation signals under different angles

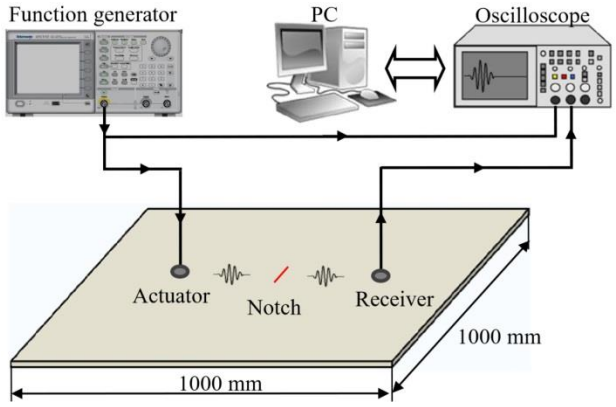

Fig. 6 Ultrasonic Lamb wave defect experimental system

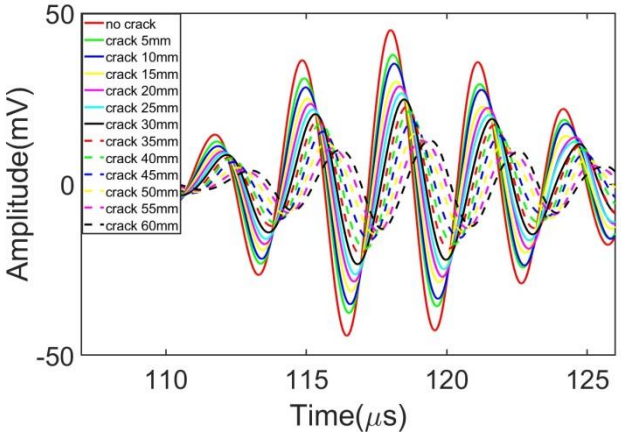

Fig. 7 Experimental results of notches with different lengths

increased from 60° to 90°, the simulated signals showed no significant change. For the 60-mm long notch (Fig. 5(b)), when the angle increased from 0° to 75°, the amplitude of simulated signals gradually decreased and the phase-shifted to the right. When the angle increased from 75° to 90°, the simulated signals showed no significant change.

2.2 Experimental Verification

In order to verify the simulation results in Section 2.1, the aluminum plate adopted in the experiment was the same to that in finite element analysis. Wire cut electrical discharge machining (WEDM) was used to machine the aluminum plate to form a through-thickness rectangular notch with a width of 0.2 mm at a center of the aluminum plate. Fig. 6 shows the schematic diagram of the experimental system composed of a digital oscilloscope Tektronix® DPO2024B, a function generator Tektronix® AFG3021B, a computer, excitation and acquisition sensors, and an aluminum plate to be inspected. The sensors are made of piezoelectric ceramics (PZT5) with a diameter of 8 mm and a thickness of 0.48 mm. The sensors were bonded to the aluminum plate with epoxy resin glue. The excitation signal is a five-cycle sinusoidal tone burst modulated by a Hanning window with a center frequency of 300 kHz. The voltage applied on the actuator is 10 V.

Firstly, the influences of notch length on detected signals were experimentally explored. The sensor arrangement (P1 and P13) is shown in Fig. 3. The notch length was increased from 0 mm to 60 mm with the step of 5 mm by WEDM. The sampling frequency was 250MHz. The acquired data were processed with the 256-time collecting and averaging method to reduce the deviation. Fig. 7 shows the detected signals for notches with different lengths after noise suppression by wavelets. With the increase in notch length, the amplitude of detected signals gradually decreased and the phase-shifted to the right. The experimental results were consistent with the above simulation results.

Then, the influences of different angles between sensing path and notch length direction on detected signals were experimentally studied. The above experimental conditions were adopted. The sensing paths are the paths (P7-P19, P6-P18, P5-P17, P4-P16, P3-P15, P2-P14 and P1-P13) shown in Fig. 3. A through-thickness notch with a width of 0.2 mm and a length of 60 mm was processed at the center of the aluminum plate by WEDM. The baseline signals and current signals were obtained at different angles and normalized(Fig. 8). When the angle increased from 0° to 75°, the current signal amplitude gradually decreased and the phase-shifted to the right compared to baseline signal. When the angle increased from 75° to 90°, the current signals showed no significant change. The experimental results were consistent with the above simulation results.

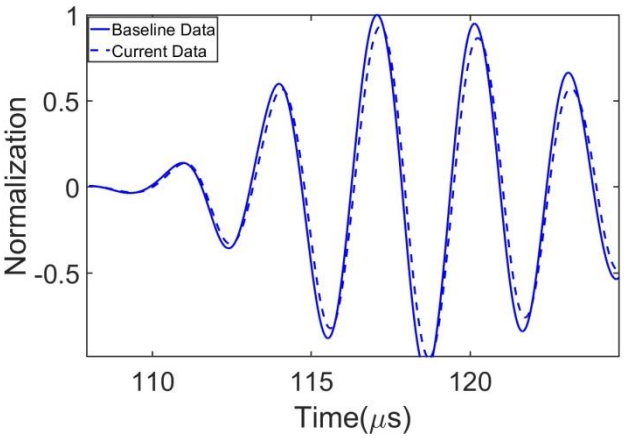

(a) Signals obtained at the angle of 0°

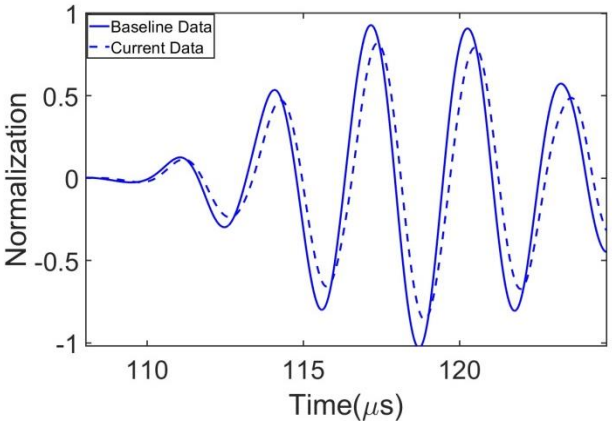

(b) Signals obtained at the angle of 15°

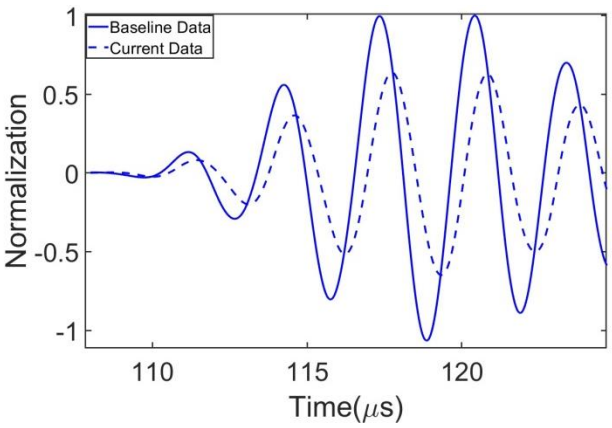

(c) Signals obtained at the angle of 30°

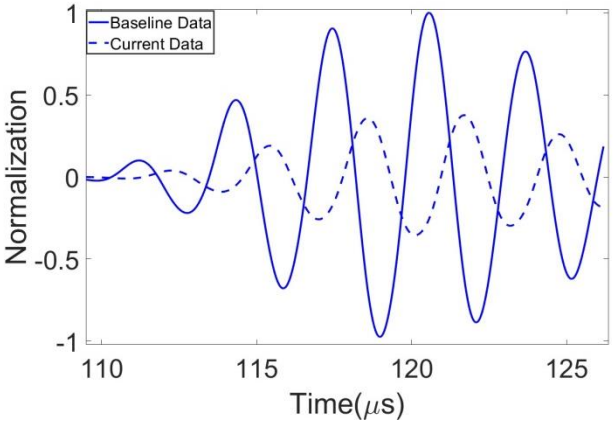

(g) Signals obtained at the angle of 90°

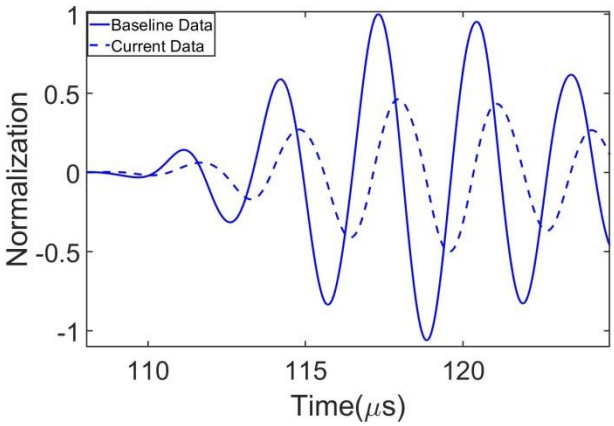

(d) Signals obtained at the angle of 45°

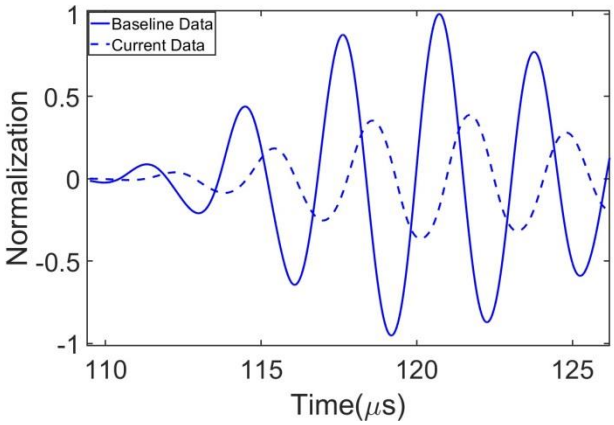

(e) Signals obtained at the angle of 60°

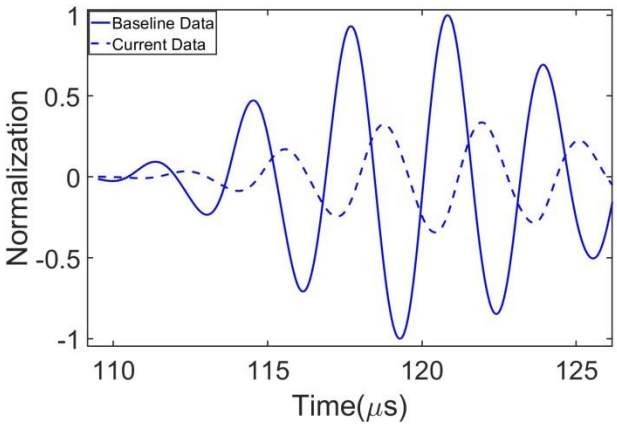

(f) Signals obtained at the angle of 75°

Fig. 8 Experimental results of different notch angles

In summary, the results of finite element analysis and experiments showed that on the sensing path vertically passing through a notch (P1-P13 in Fig. 3), as the notch length increased, the signal amplitude decreased and the phase-shifted to the right. The above changes of received signals might be interpreted as follows. The two sides of the through-thickness notch were completely separated from each other and the signals received by sensors were diffracted from the notch tip. With the increase in the propagation distance, amplitude attenuation was enhanced

and time of flight was delayed. Similarly, with the increase in the angle between the sensing path and the notch length direction, the distance from the notch tip to the reception point increased. Therefore, the signal amplitude decreased and the phase-shifted to the right. However, after the angle increased above a certain value, the propagation distance showed no significant change, so the signal change was no longer obvious.

3. Notch Identification and Evaluation Methods

3.1 Calculation method of damage index

In the detection process, if there is a damage on the sensing path, damaged signals will be different from healthy signals. The degree of the difference is represented by damage index (DI). According to the analysis in Section 2, the amplitude and phase of detected signals varied with notch length. Therefore, a damage index calculation method is proposed as:

$$DI = 1 - \frac{\sum (x_i - \bar{x})(y_i - \bar{y})}{\sum (x_i - \bar{x})^2} \tag{4}$$

where x_i indicates baseline signals; $\bar{x}$ indicates an average value of baseline signals; y_i indicates current signals; $\bar{y}$ indicates an average value of current signals. DI ranges from 0 to 2. When DI is 0, the subtraction is 1, indicating that the deviations of current signals and baseline signals from their means are exactly the same and that the two waveforms are basically the same. When DI is 2, the subtraction is -1, indicating that the current signals are opposite to baseline signals and that the difference is the greatest.

In Eq. (4), the numerator represents the degree of the change in the same direction of two variables and the denominator is the standard deviation of baseline signal and describes the magnitude of deviation from its mean. The calculation eliminates the effect of amplitude variation of the baseline signal and reflects the amplitude and phase changes. The proposed method can better reflect the damage characteristics of a notch.

3.2 Notch direction identification method

With the damage index calculation method proposed in Section 3.1, DI values of simulation and experimental signals at different angles between sensing path and notch length direction in Section 2 were calculated. Fig. 9 shows the DI variations for two notches (30 mm and 60 mm long). Table 2 and Table 3 respectively show the DI of simulation signals of the two notches under different angles.

With the increase in the angle between sensing path and notch length direction, the damage index increased (Fig. 9), but the increasing trend was not significant when the angle increased to a certain value. Therefore, it was impossible to determine whether the sensing path corresponding to the maximum DI was perpendicular to the notch length direction. Since the Lamb wave propagation path was symmetrical with respect to the notch,

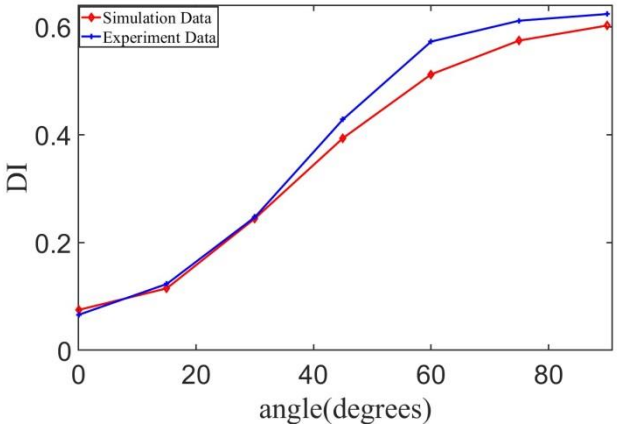

(a) DI distribution for a 30-mm long notch

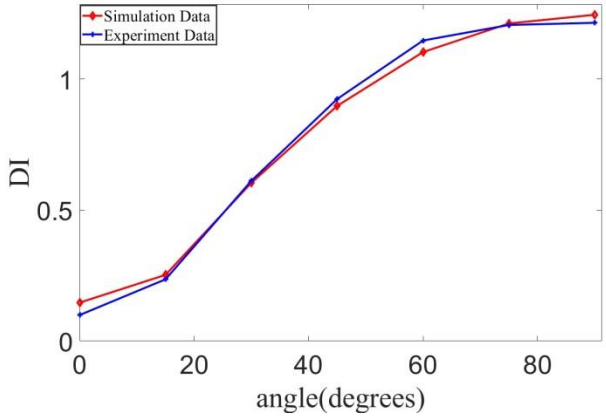

(b) DI distribution for a 60-mm long notch

Fig. 9 DI of simulation and experimental signals at different angles

Table 2 DI of simulation signals under different angles for a 30-mm long notch

Angles(°)	DI1	Angles(°)	DI2	|DI1-DI2|
0	0.0748	90	0.6023	0.5275
15	0.1148	105	0.5744	0.4596
30	0.2443	120	0.5117	0.2674
45	0.3935	135	0.3935	0
60	0.5117	150	0.2443	0.2674
75	0.5744	165	0.1148	0.4596
90	0.6023	180	0.0748	0.5275

Table 3 DI of simulation signals under different angles for a 60-mm long notch

Angles(°)	DI1	Angles(°)	DI2	|DI1-DI2|
0	0.1466	90	1.2452	1.0986
15	0.2525	105	1.2120	0.9595
30	0.6041	120	1.1029	0.4988
45	0.8976	135	0.8976	0
60	1.1029	150	0.6041	0.4988
75	1.2120	165	0.2525	0.9595
90	1.2452	180	0.1466	1.0986

a damage index of the sensing path perpendicular to the angle between sensing path and notch length direction could be obtained. Among the absolute values of the damage index differences of any two perpendicular paths passing through the notch, the absolute value of the damage index difference between the two paths which are respectively perpendicular and parallel to the notch length direction is the largest (Tables 2-3). Therefore, it can be considered that when the absolute value of the damage index difference between two sensing paths perpendicular to each other is the largest, the path direction in which the damage index is smaller is the notch direction.

The area with potential notches should be calculated before notch evaluation. The RAPID was used in this study. The DI of each sensing path in the sensor network was calculated by the damage index calculation method proposed in Section 3.1. Then the effective influencing area of every sensing path was determined by the weighted distribution function and the damage probabilities of all the points in the detected area under the influences of all sensing paths were calculated. The position with the largest damage probability was the position where the notch might exist. The weighted distribution function is expressed as follows (Lee *et al*. 2015)

$$m_{ij}(x,y)=\begin{cases}1-\dfrac{R_{ij}(x,y)}{\beta} & R_{ij}(x,y)\langle\beta \\ 0 & R_{ij}(x,y)\geq\beta\end{cases} \tag{5}$$

where β is a shape factor determining the size of the area affected by the damage index on the sensing direct path and its value is less than 1; $R_{ij}(x,y)$ indicates the ratio of the sum of the distances from any point (x_k, y_k) to the excitation sensor (x_{ik}, y_{ik}) and the acquisition sensor (x_{kj}, y_{kj}) to the sensing path (the distance between the excitation sensor and the acquisition sensor) minus 1(Zhao *et al*. 2007, Wang *et al*. 2010):

$$R(x_k,y_k,x_{ik},y_{ik},x_{kj},y_{kj})=\left(\frac{\sqrt{(x_k-x_{ik})^2+(y_k-y_{ik})^2}}{\sqrt{(x_{ik}-x_{kj})^2+(y_{ik}-y_{kj})^2}}+\frac{\sqrt{(x_k-x_{kj})^2+(y_k-y_{kj})^2}}{\sqrt{(x_{ik}-x_{kj})^2+(y_{ik}-y_{kj})^2}}\right)-1 \tag{6}$$

In a sensor network composed of N piezoelectric transducers, the damage probability at any point (x, y) in the detected area under the influence of all sensing paths is expressed as (Liu *et al*. 2015, Wang *et al*. 2010):

$$P(x,y)=\sum_{i=1}^{N-1}\sum_{j=i+1}^{j=N}DI_{ij}m_{ij}(x,y) \tag{7}$$

The principle of notch direction identification is shown in Fig. 10. In the sensor network composed of N piezoelectric transducers, there are a total of N (N-1) sensing paths, which are divided into N groups as excitation sensors. Firstly, the sensing path with the largest damage index in each group is calculated and selected, and then the largest n (n<N) damage index values and their

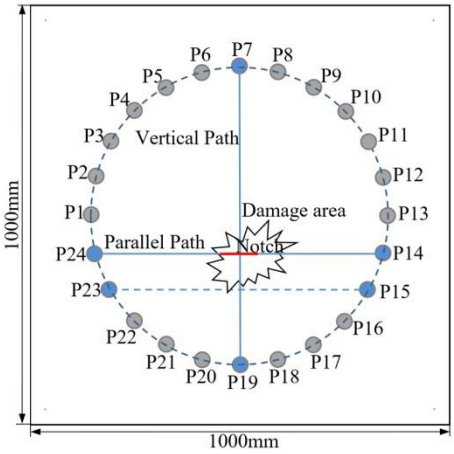

Fig. 10 Principle of notch direction identification

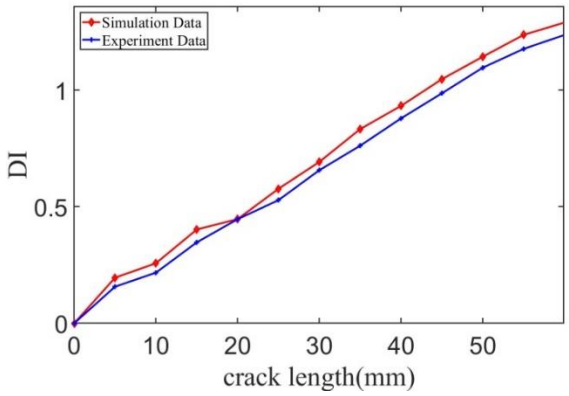

Fig. 11 DI of simulation and experimental signals at different lengths

corresponding sensing paths are found from the N largest damage index values. The found sensing paths are possibly perpendicular to the notch direction. Then the paths which are perpendicular to the n paths and pass through the possible area of the notch are obtained. If two or more paths are perpendicular to any one of n paths and pass through the area, the path with the largest damage index is determined as the desired path because the paths with smaller DI values may not pass through the notch. Then, in the obtained n sets of two mutually perpendicular paths, the absolute values of the DI differences in each group of two mutually perpendicular paths are calculated. The two mutually perpendicular paths in the group with the maximum absolute value of the DI difference are respectively the vertical (DI larger path) and parallel (DI smaller path) directions of the notch.

3.3 Notch Location and Length Evaluation Methods

With the method proposed in Section 3.1, DI values of simulation and experimental signals under notches with different lengths in Section 2 were calculated (Fig. 11). With the increase in notch length, the DI values showed a monotonous increase trend and the DI values of simulation signals were well consistent with those of experimental signals.

According to the geometric principle, with the known

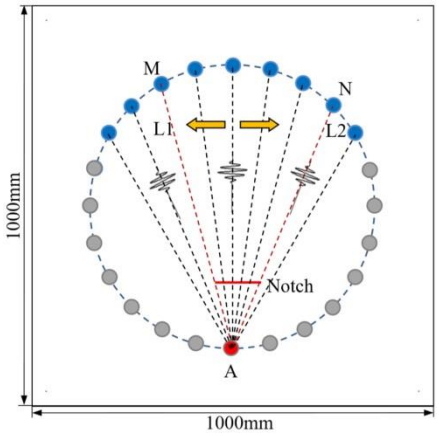

Fig. 12 Principle of notch length determination

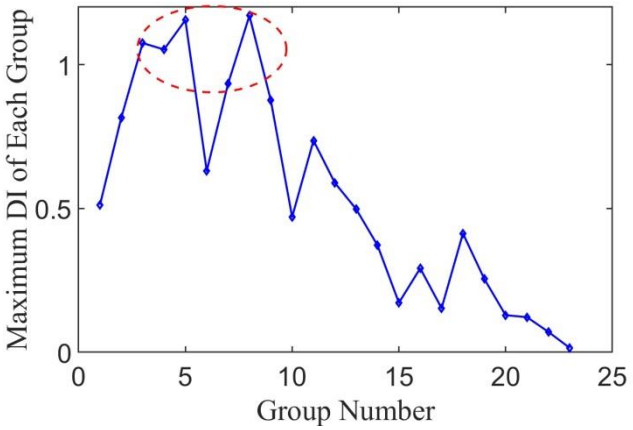

Fig. 13 Maximum DI values of each group

notch direction, if a certain point of the notch is determined, the equation of the straight line where the notch is located can be obtained. We believed that in the damage distribution obtained by the RAPID, the point with the highest damage probability was the point at which the notch passes. Therefore, the coordinate points whose damage probabilities are higher than the threshold (such as 99.99%) were averaged as one point of the notch.

When the sensing path passes through the notch and is perpendicular to the notch length direction, the difference between the current signal and the baseline signal is large, thus resulting in a large damage index of the sensing path. If the sensing path does not pass through the notch, the corresponding damage index is relatively small. Therefore, the notch length can be estimated based on the damage index distribution along sensing paths that have the same actuator. In the sensing path perpendicular to the notch obtained in Section 3.2, the sensor which is closer to the line where the notch is located in the actuator and the other sensors are acquisition sensors, as shown in Fig. 12. With the acquisition sensor perpendicular to the notch as the center, the damage index larger than the threshold and corresponding acquisition sensors is checked from both sides of the center. Based on the notch tip effect and multiple test results, the threshold of the damage index is set to be 0.4. Then two lines L1 and L2 can be determined with the actuator A and the two critical acquisition sensors (M and N). The intersection between the two straight lines and the line where the notch is located in the two tips of the notch. Then the notch length can be determined.

4. Experimental Verification

The above notch identification and evaluation methods were experimentally verified. The same test conditions in Section 2.2 and the sensor arrangement is shown in Fig. 3 were set in the experiment. The 24 piezoelectric transducers were evenly arranged along a circle centered at the center of the aluminum plate and having a radius of 200 mm. The through-thickness notch was 50 mm long and located on the line connecting the sensors 15 and 23.

During the experiment, each sensor acted as an actuator and the remaining sensors acquired signals. Since ultrasonic guided wave propagation is reversible, the two Lamb wave signals acquired between a pair of sensing units, regardless of which one was the actuator, showed considerable similarity. Therefore, there are 276 sensing paths in the sensor network composed of 24 sensors. The adopted excitation waveform was a five-cycle sinusoidal tone burst modulated by a Hanning window with a center frequency of 300 kHz. Baseline signals and current signals were respectively acquired. According to different actuators, the detection signals were divided into 23 groups and the damage index was calculated with Eq. (4). The maximum value of each group was selected (Fig. 13). The top five maximum DI values in Fig. 13 were further selected and corresponding sensing paths perpendicular to and passing through the notch were found (Table 4). Among 5 groups of the two mutually vertical paths, the path 5-20 and path 14-23 showed the largest absolute value of damage index difference. Therefore, the notch direction was considered to be perpendicular to the sensing path 5-20.

Table 4 Notch direction determination parameters

Ex1	Re1	DI1	Ex2	Re2	DI2	|DI1-DI2|
8	21	1.1704	17	24	0.3846	0.7858
5	20	1.1550	14	23	0.2585	0.8965
3	19	1.0750	12	22	0.5891	0.4859
4	20	1.0526	14	22	0.3716	0.6810
7	21	0.9336	16	24	0.2919	0.6417

The RAPID method was used to calculate the point with the highest damage probability. As marked by the yellow point in Fig. 14, the red line is the true notch. The calculated point was basically coincident with the notch. Based on the direction of the notch and the passing point, the equation of the line where the notch was located was obtained. With the sensor 20, which was perpendicular to the notch and the closest to the line where the notch was located, as the actuator, the damage index of the remaining sensors was plotted (Fig. 15). The sensors whose damage index was greater than a threshold were found on both sides of the vertical acquisition sensor 5. The damage index corresponding to the acquisition sensors 2 and 7 was greater than a threshold of 0.4. Two virtual positions with a damage index of 0.4 were calculated and respectively connected to

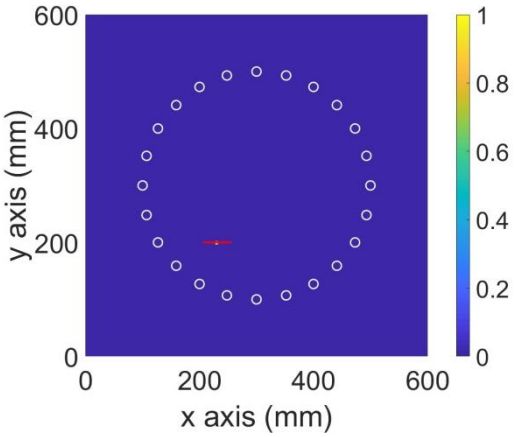

Fig. 14 Points through which the notch passes

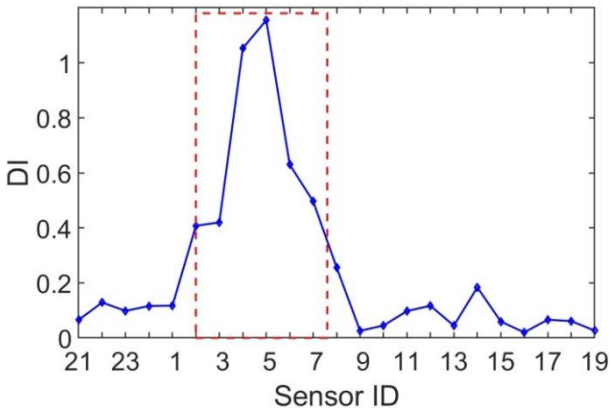

Fig. 15 DI Distribution of all acquisition sensors by actuator 20

Table 5 Comparison of detected notch angles and actual notch angles

Actual notch angles (°)	Detected notch angles (°)	Errors (°)	Errors (%)
0	7.47	7.47	2.08
333.43	330.03	3.40	1.02
90	90	0	0
51.07	45	6.07	11.89

the sensor 20 and the notch length was calculated to be 56.87 mm by the geometric method. The notch imaging is shown in Fig. 16(a). The red line indicates a true notch, whereas the black line indicates the calculated notch.

According to the same detection and evaluation methods, the notches of different directions and different lengths were experimentally explored. The results are shown in Tables 5-6. The notch imaging result is shown in Figs. 16(b)-(d).

The methods were more accurate in estimating the notch direction and location. However, the maximum error of the evaluated notch length was 21.19%. The angular error was related to the number of sensors. The more sensors allowed the denser sensing paths and the smaller angular error. The notch length error was mainly ascribed to the mode conversion when excitation signals were transmitted to the notch tip. Therefore, it was not easy to determine notch tips.

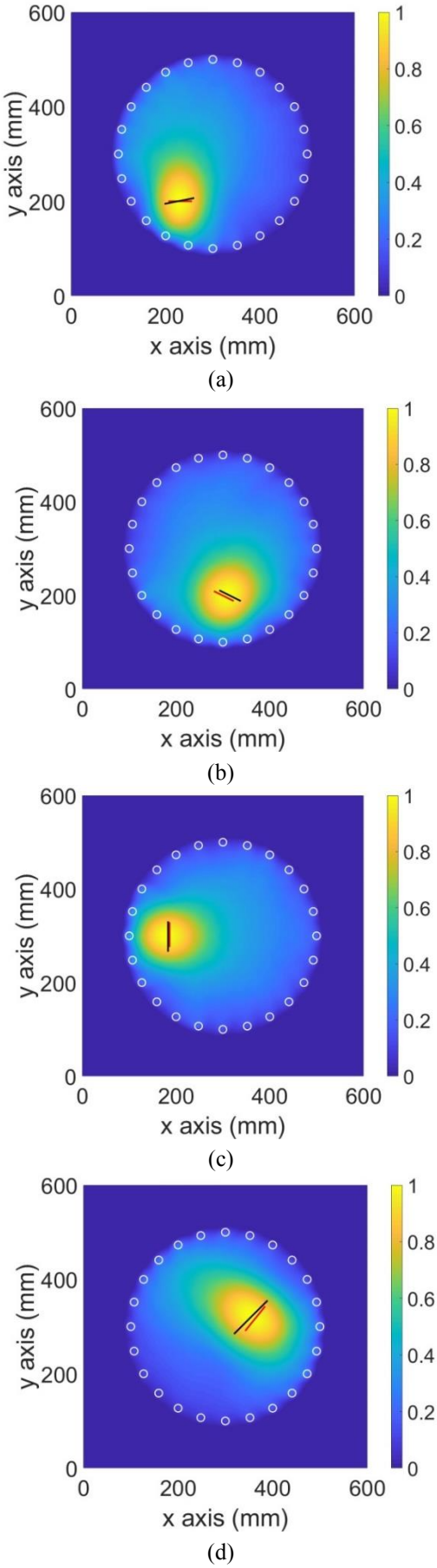

Fig. 16 Notch imaging

Table 6 Comparison of detected notch lengths and actual notch lengths

Actual notch lengths (mm)	Detected notch lengths (mm)	Errors (mm)	Errors (%)
50	56.87	6.87	13.74
45	49.83	4.83	10.73
55	61.99	6.99	12.71
67	81.20	14.20	21.19

5. Conclusions

In this study, the through-thickness rectangular notch detection and evaluation method were proposed. Through finite element analysis and experiments, we found that when the sensing path passed through a notch, as the notch length increased, the signal amplitude decreased and the phase-shifted to the right. Similarly, with the increase in the angle between the sensing path and the notch length direction, the similar changes in signal amplitude and phase were observed. Then a damage index calculation method for through-thickness notches was proposed. The method could comprehensively reflect the amplitude and phase changes of detected signals caused by notches. Based on the damage index difference between two vertically crossed sensing paths that passed through the notch, the notch direction identification method was proposed. The notch length was determined based on the damage index distribution along sensing paths. The proposed method was experimentally verified. The comparison between the values of detected notch angles and actual notch angles showed that the error deviation was less than 12%. However, the maximum error of evaluated notch length was higher than 20%. In the future, further studies will be conducted to achieve the accurate evaluation of notch length.

Acknowledgments

This work was supported by the National Key Research and Development Program of China [grant no. 2016YFF0203002].

References

Avazpour, L. (2018), "Fractional Ostrowski type inequalities for functions whose derivatives are prequasiinvex", *J. Inequalities Special Funct.*, **9**(2), 15-29. https://doi.org/10.22342/jims.1.1.751.%25p.

Avazpoura, L., Allahviranloob, T., and Islamc, S. (2016), "Uncertain Hermite-Hadamard inequality for functions with (s, m)- Godunova-Levin derivatives via fractional integral", *J. Nonlinear Sci. Appl.*, **9**(5),3333--3347 http://dx.doi.org/10.22436/jnsa.009.05.119.

Cao, M., Ostachowicz W., Radzieński, M., Xu, W. (2013), "Multiscale shear-strain gradient for detecting delamination in composite laminates", *Appl. Phys. Lett.*, **103**(10): 101910. https://doi.org/ 10.1063/1.4820182.

Delkhosh, M., Parand, K., and Ganji, D.D. (2018), "An efficient numerical method to solve the Falkner-Skan problem over an isothermal moving wedge", *J. Numeric. Method. Heat Fluid Flow*, **28**(9), 2132-2157. https://doi.org/10.1108/hff-11-2017-0480.

Deraemaeker, A., Preumont A., Reynders, E., De R. G., Kullaa, J., Lamsa, V., Worden, K., Manson, G., Barthorpe, R., Papatheou, E., Kudela, P., Malinowski, P., Ostachowicz, W. and Wandowski, T. (2010), "Vibration-based structural health monitoring using large sensor networks", *Smart Struct. Syst.*, **6**(3), 335-347. https://doi.org/10.12989/sss.2010.6.3.335.

Fan, G., Zhang, H., Zhang, H., Zhu, W. and Chai, X. (2018), "Lamb wave local wavenumber approach for characterizing flat bottom defects in an isotropic thin plate", *Appl. Sci.*, **8**(9), 1600. https://doi.org/10.3390/app8091600.

Ghadami, A., Behzad, M. and Mirdamadi, H. R. (2015), "A mode conversion-based algorithm for detecting rectangular notch parameters in plates using Lamb waves", *Arch. Appl. Mech.*, **85**(6), 793-804. https://doi.org/10.1007/s00419-015-0991-x.

Hashemiparast, S. M., and Avazpour, L. (2008), "Applying Quadrature Rules with Multiple Nodes to Solving Integral Equations", *AIP Conference Proceedings*, **1048**(1), 257-260. https://doi.org/10.1063/1.2990906.

He, J., Ran, Y., Liu, B., Yang, J. and Guan, X. (2017), "A fatigue crack size evaluation method based on Lamb wave simulation and limited experimental data", *Sensors*, **17**(9), 2097. https://doi.org/10.3390/s17092097.

Hong, M., Wang, Q., Su, Z. and Cheng, L. (2014), "In situ health monitoring for bogie systems of CRH380 train on Beijing–Shanghai high-speed railway", *Mech. Syst. Signal Process.*, **45**(2), 378-395. https://doi.org/10.1016/j.ymssp.2013.11.017.

Huang, S., Wei, Z., Zhao, W. and Wang, S. (2014), "A new omni-directional EMAT for ultrasonic Lamb wave tomography imaging of metallic plate defects", *Sensors*, **14**(2), 3458-3476. https://doi.org/10.3390/s140203458.

Ihn, J. B. and Chang, F. K. (2004), "Detection and monitoring of hidden fatigue crack growth using a built-in piezoelectric sensor/actuator network: I. Diagnostics", *Smart Mater. Struct.*, **13**(3), 609-620. https://doi.org/10.1088/0964-1726/13/3/020.

Jamshidi, L., and Avazpour, L. (2012), "Solution of the fuzzy boundary value differential equations under generalized differentiability by shooting method", *J. Fuzzy Set Value Anal.*, Article ID jfsva-00136, http://dx.doi.org/10.5899/2012/jfsva-00136**.**

Lee, B. C. and Staszewski, W. J. (2003), "Modelling of Lamb waves for damage detection in metallic structures: Part I. Wave propagation", *Smart Mater. Struct.*, **12**(5), 804-814. https://doi.org/10.1088/0964-1726/12/5/018.

Lee, J., Sheen, B. and Cho, Y. (2015), "Quantitative tomographic visualization for irregular shape defects by guided wave long range inspection", *J. Precision Eng. Manufact.*, **16**(9), 1949-1954. https://doi.org/10.1007/s12541-015-0253-4.

Liu, Z., Feng, X., He, C., and Wu, B. (2018), "Quantitative rectangular notch detection of Laser-induced Lamb waves in aluminium plates with wavenumber analysis", *Trans. Nanjing U Aeronautics Astronautics*, **2**, 244-255. https://doi.org/10.16356/j.1005-1120.2018.02.244.

Liu, Z., Yu, H., Fan, J., Hu, Y., He, C. and Wu, B. (2015), "Baseline-free delamination inspection in composite plates by synthesizing non-contact air-coupled Lamb wave scan method and virtual time reversal algorithm", *Smart Mater. Struct.*, **24**(4), https://doi.org/10.1088/0964-1726/24/4/045014 .

Lowe, M. J. S. and Diligent, O. (2002b), "Low-frequency reflection characteristics of the s0 Lamb wave from a rectangular notch in a plate", *J. Acoustical Soc. America,* **111**(1), 64-74. https://doi.org/10.1121/1.1424866.

Lowe, M. J. S., Cawley, P., Kao, J. Y. and Diligent, O. (2002a), "The low frequency reflection characteristics of the fundamental antisymmetric Lamb wave a0 from a rectangular notch in a

plate", *J. Acoustical Soc. America*, **112**(6), 2612-2622. https://doi.org/10.1121/1.1512702.

Lu, G., Feng, Q., Li, Y., Wang, H. and Song, G. (2017), "Characterization of ultrasound energy diffusion due to small-size damage on an aluminum plate using piezoceramic transducers", *Sensors*, **17**(12), 2796. https://doi.org/10.3390/s17122796.

Lu, Y., Ye, L. and Su, Z. (2006), "Crack identification in aluminium plates using Lamb wave signals of a PZT sensor network", *Smart Mater. Struct.*, **15**(3), 839-849. https://doi.org/10.1088/0964-1726/15/3/021.

Lu, Y., Ye, L., Su, Z. and Huang, N. (2007), "Quantitative evaluation of crack orientation in aluminium plates based on Lamb waves", *Smart Mater. Struct.*, **16**(5), 1907-1914. https://doi.org/10.1088/0964-1726/16/5/047.

Lu, Y., Ye, L., Su, Z. and Yang, C. (2008), "Quantitative assessment of through-thickness crack size based on Lamb wave scattering in aluminium plates", *Ndt and E International*, **41**(1), 59-68. https://doi.org/10.1016/j.ndteint.2007.07.003.

Marino-Merlo, E., Bulletti, A., Giannelli, P., Calzolai, M. and Capineri, L. (2018), "Analysis of Errors in the Estimation of Impact Positions in Plate-Like Structure through the Triangulation Formula by Piezoelectric Sensors Monitoring", *Sensors*, **18**(10), 3426. https://doi.org/10.3390/s18103426.

Moser, F., Jacobs, L. J. and Qu, J. (1999), "Modeling elastic wave propagation in waveguides with the finite element method", *Ndt and E International*, **32**(4), 225-234. https://doi.org/10.1016/S0963-8695(98)00045-0.

Ng, C.(2015), "A two-stage approach for quantitative damage imaging in metallic plates using Lamb waves", *Earthq. Struct.*, **8**(4), 821-841. https://doi.org/10.12989/eas.2015.8.4.821.

Rao, J., Ratassepp, M., Lisevych, D., Hamzah Caffoor, M. and Fan, Z. (2017), "On-line corrosion monitoring of plate structures based on guided wave tomography using piezoelectric sensors", *Sensors*, **17**(12), 2882. https://doi.org/10.3390/s17122882.

Rose, J. L. (2002), "A baseline and vision of ultrasonic guided wave inspection potential", *J. Pressure Vessel Technol.*, **124**(3), 273-282. https://doi.org/10.1115/1.1491272.

Rucka, M., Wojtczak, E. and Lachowicz, J. (2018), "Damage imaging in Lamb wave-based inspection of adhesive joints", *Appl. Sci.*, **8**(4), 522. https://doi.org/10.3390/app8040522.

Samaee, S. S., Yazdanpanah, O., Ganji, D. D., and Mofidi, A. A. (2015), "Analytical solution for a suspension bridge by applying HPM and VIM", *J. Comput. Math.*, 92(4), 782-801. https://doi.org/10.1080/00207160.2014.909929.

Santos, M. J., Perdigao, J. and Faia, P. (2008), "Ultrasonic guided waves scattering effects from defects in adhesively bonded lap joints using pitch and catch and pulse-echo techniques", *J. Adhesion*, **84**(5), 421-438. https://doi.org/10.1080/00218460802089262.

Sen, D., Nagarajaiah, S. and Gopalakrishnan, S. (2017), "Harnessing sparsity in lamb wave-based damage detection for beams", *Struct. Monitor. Maintenance*, **4**(4), 381-396. https://doi.org/10.12989/smm.2017.4.4.381.

Sohn, Y. and Krishnaswamy, S. (2004), "Interaction of a scanning laser-generated ultrasonic line source with a surface-breaking flaw", *J. Acoustical Soc. America*, **115**(1), 172-181. https://doi.org/10.1121/1.1630997.

Su, Z., Ye, L. and Lu, Y. (2006), "Guided Lamb waves for identification of damage in composite structures: A review", *J. Sound Vib.*, **295**(3-5), 753-780. https://doi.org/10.1016/j.jsv.2006.01.020.

Van Velsor, J. K., Gao, H. and Rose, J. L. (2007), "Guided-wave tomographic imaging of defects in pipe using a probabilistic reconstruction algorithm", *Insight Non Destructive Test. Condition Monitor.*, **49**(9), 532-537. https://doi.org/10.1784/insi.2007.49.9.532.

Wang, D., He, J., Guan, X., Yang, J. and Zhang, W. (2018), "A model assessment method for predicting structural fatigue life using Lamb waves", *Ultrasonics*, **84**, 319-328. https://doi.org/10.1016/j.ultras.2017.11.017.

Wang, D., Ye, L., Lu, Y. and Li, F. (2010), "A damage diagnostic imaging algorithm based on the quantitative comparison of lamb wave signals", *Smart Mater. Struct.*, **19**(6), 065008. https://doi.org/10.1088/0964-1726/19/6/065008.

Wang, Q. and Xu, J. (2014), "Lamb wave tomography technique for crack damage detection", *Proceedings of the 33rd Chinese Control Conference*, Nanjing, China, July.

Wang, Q., Wang, M., Yue, D. and Su, Z. (2016), "A Lamb wave-based crack diagnosis method using an improved RAPID algorithm", *Proceedings of the 8th European Workshop On Structural Health Monitoring*, Bilbao, Spain, July.

Xu, W., Cao, M., Ostachowicz, W., Radzieński, M. and Xia, N. (2015), "Two-dimensional curvature mode shape method based on wavelets and Teager energy for damage detection in plates", *J. Sound Vib.*, **347**, 266-278. https://doi.org/10.1016/j.jsv.2015.02.038.

Xu, W., Ding, K., Liu, J., Cao, M., Radzieński, M. and Ostachowicz, W. (2019a), Non-uniform crack identification in plate-like structures using wavelet 2D modal curvature under noisy conditions. *Mech. Syst. Signal Process.*, **126**, 469-489. https://doi.org/10.1016/j.ymssp.2019.01.047.

Xu, W., Radzieński, M., Ostachowicz, W. and Cao, M. (2013), "Damage detection in plates using two-dimensional directional Gaussian wavelets and laser scanned operating deflection shapes", *Struct. Health Monitoring*, **12**(5-6), 457-468. https://doi.org/10.1177/1475921713492365.

Xu. W., Fang. H., Cao. M., Zhou. L., Wang. Q., and Ostachowicz. W. (2019b), "A noise-robust damage indicator for characterizing singularity of mode shapes for incipient delamination identification in CFRP laminates", *Mech. Syst. Signal Process.*, **121**, 183-200. https://doi.org/10.1016/j.ymssp.2018.10.025

Yan, F., Royer Jr, R. L. and Rose, J. L. (2010), "Ultrasonic guided wave imaging techniques in structural health monitoring", *J. Intelligent Mater. Syst. Struct.*, **21**(3), 377-384. https://doi.org/10.1177/1045389X09356026.

Yang, J., He, J., Guan, X., Wang, D., Chen, H., Zhang, W. and Liu, Y. (2016), "A probabilistic crack size quantification method using in-situ Lamb wave test and Bayesian updating", *Mech. Syst. Signal Process.*, **78**, 118-133. https://doi.org/10.1016/j.ymssp.2015.06.017.

Zhao, X., Gao, H., Zhang, G., Ayhan, B., Yan, F., Kwan, C. and Rose, J. L. (2007), "Active health monitoring of an aircraft wing with embedded piezoelectric sensor/actuator network: I. Defect detection, localization and growth monitoring", *Smart Mater. Struct.*, **16**(4), 1208-1217. https://doi.org/10.1088/0964-1726/16/4/032.

CC